JCTC Journal of Chemical Theory and Computation

The Dissociated Amorphous Silica Surface: Model Development and Evaluation

Ali A. Hassanali,[†] Hui Zhang,[‡] Chris Knight,[‡] Yun Kyung Shin,[‡] and Sherwin J. Singer*[,†,‡]

Biophysics Program, and Department of Chemistry, Ohio State University, Columbus, Ohio 43210, United States

Received May 17, 2010

Abstract: At pH 7, amorphous silica has a characteristic negative charge due to the deprotonation of silanol groups on the surface. Electrokinetic phenomena and transport of biomolecules in devices depend sensitively on the surface morphology, distribution of ions and solvent, and adsorption properties of solutes close to the surface in the electrical double layer region. Hence, simulation of these phenomena requires detailed atomistic models of the double layer region. In this Article, we extend our undissociated silica surface model [*J. Phys. Chem. B* **2007**, *111*, 11181−11193] to include dissociated $Si-O^-$ groups, which interact with both water and salt (Na^+ and Cl^-). We have also conducted ab initio molecular dynamics (AIMD) simulations of a smaller system consisting of a hydrated silica slab. The radial distribution functions predicted by the empirical model are in qualitative agreement with those from the AIMD simulations. The hydrophobic and hydrophilic nature of silanol-poor and silanol-rich regions of the amorphous silica surface observed in our empirical model is reproduced in the AIMD simulations of the smaller slab. In the initial stages of our AIMD simulations, we observe various chemical processes that represent different hydroxylation mechanisms of the surface.

1. Introduction

Interfaces between amorphous silica and water are ubiquitous in chemical, biochemical, and environmental settings.[1,2] The strong interactions between silica, water, and adsorbates, such as biomolecules,[3] make the amorphous silica surface an important and challenging system to model. These strong interactions between silica and analytes are often exploited in chromatographic applications.[4,5] The interaction of silica and biomolecules is important in several arenas. Silica−DNA interactions are the basis of a standard purification scheme for nucleic acids[6,7] and novel microfabricated device applications.[8,9] There has been recent interest in using silica nanochannels to stretch and sequence DNA.[10,11] Silicates and silica exhibit widely varying health effects, with considerable effort devoted to elucidating mechanisms of toxicity.[3,12] The importance of biomolecules at the water−silica interface in a variety of situations has prompted a number of fundamental investigations of the interactions of silica with nucleic acids[13−19] and proteins.[20−23] In addition to devices fabricated from silica, the amorphous silica−water interface is important in silicon-based devices where silicon acquires an oxide coating in contact with aqueous solution.[24,25] At all but the lowest pH values, a silica surface in contact with water is negatively charged. Electrochemical and electrokinetic function of numerous practical devices depends not only on the overall surface charge, but also on the detailed microscopic properties of the silica−water interface. This is because the driving force for electroosmotic flow (EOF), even in fluidic channels of large dimension, originates in the electric double layer,[26] the region of excess charge in the fluid that compensates the surface charge. Most of the excess charge of the double layer is typically located within a nanometer from the surface. There is a need for interaction potential models that can describe this region with some realism, and yet will be tractable for simulations that cover large spatial and time scales.

* Corresponding author e-mail: singer@chemistry.ohio-state.edu.
[†] Biophysics Program.
[‡] Department of Chemistry.

10.1021/ct100260z
Published on Web 10/11/2010

Recently, we have developed a model for the undissociated amorphous silica interface.[27−29] In this Article, we describe an extension to that model to include dissociated silanol groups on the surface. The negative charge that develops at the water−silica interface arises from the deprotonation of silanol groups. As one illustration of the applications of this work, we have recently applied the model described herein to study electrokinetic phenomena.[30] Using nonequilibrium molecular dynamics (MD) simulations of aqueous solvent containing Na^+ and Cl^- ions near a realistically modeled surface, we have critically evaluated the classical Gouy−Chapman−Stern model[31−34] and the dynamic Stern layer model,[35−43] used extensively to account for surface ion conduction. The heat of immersion calculated with our model for the undissociated surface is in good agreement with available experimental data.[28] Silanol densities typical of common silica materials naturally arose in our annealing and hydroxylating procedure.[28] Further calibration of the accuracy of this model, as extended in this work, is supplied in the form of comparisons with ab initio molecular dynamics (AIMD) simulations.

Feuston and Garofalini[44,45] have developed an empirical potential for the water−amorphous silica interface. In their model, which has been applied and extended,[46−49] the silicon, oxygen, and hydrogen atoms are not fixed to any molecular unit such as a silanol or water group, but instead can spatially evolve over the course of the simulation based on the interaction potential. Garofalini and co-workers have recently developed an improved dissociative water potential for molecular dynamics simulations[50] and have applied it to study the chemisorption of water on silica surfaces, yielding important insights into the surface chemistry of water near silica.[48,49,51,52] To our knowledge, the applicability of this model to dissociated silica surfaces has not been assessed. Rustad and Hay[53] have also developed a dissociated model that yields reasonable acid dissociation energies for orthosilicic acid in the gas and aqueous phase. The applicability of this model for very large-scale simulations needed for device applications is however limited. Extending previous work for silicon/silicon oxide systems,[54] van Duin and coworkers have developed a dissociating force field for the silica−water system[55] using the ReaxFF force field method.[56]

Schulten and co-workers[57] have quite recently developed an empirical potential for the water−amorphous silica interface. Their model is exclusively for water interacting with a rigid silica prepared using other models. Their intended fitting procedure was to choose interaction parameters to match the water contact angle reported for quartz surface as a function of the degree of hydroxylation.[58] The parameters for their surface without silanol groups were adjusted to reproduce the water contact angle for the corresponding quartz surface. Schulten and co-workers report that their model could not reproduce the experimental contact angles of Lamb and Furlong[58] for any finite degree of hydroxylation. However, contact angle measurements at low degrees of hydroxylation are difficult because the dehydroxylated surface rapidly reacts with water, and other measurements report very different contact angles for dehydroxylated silica.[59] Jenkins and co-workers[60−62] simulated amorphous silica nanoparticles in water starting with initial configurations obtained from DMOL3[63] calculations. The simulation was then continued using empirical potentials from the OPLS-AA force field[64] and borrowed from a simulation of the quartz surface.[65] Puibasset and Pelenq have modeled the adsorption of water in mesoporous silica from submonolayer coverage to saturation pressures using grand canonical Monte Carlo simulations.[66−70] Treatment of quartz surfaces involves similar atom types, but as compared to silica is considerably simplified by the regularity of the quartz surface. MacKerell and co-workers[71] have developed a model for the quartz−water interface, which is not designed to characterize dissociated silanol groups. Freund[72] and Qiao and Aluru[73,74] have studied electrokinetic transport in electrokinetic channels where the negative charge is distributed on Lennard-Jones wall particles. In these simple models, the heterogeneity and surface roughness are not captured. Aluru and co-workers have also performed similar studies for the interface between water and a more realistic, electrically neutral quartz surface.[75] Lorenz et al.[76,77] have employed a modified version of the silica−water potential developed by Schulten and co-workers[57] to study charge inversion in the presence of divalent cations and electrokinetic phenomena associated with mono- and divalent cations.

In addition to developing an empirical potential, we have used ab initio molecular dynamics (AIMD) simulations in this work, to test several features of our empirical model, including the strong variability in relative hydrophobicity/hydrophilicity[78] with surface silanol density reported in our earlier work.[27,28] The physisorption and chemisorption of small numbers of water molecules near silica has also been examined previously by ab initio methods. Physisorption has been studied using quantum chemical fragment calculations by Saengsawang et al.[81] Cheng et al. studied the reaction of an SiO_2 molecule in a cluster with up to six water molecules.[82] Sutton and co-workers have studied the hydroxylation mechanisms of different silica clusters with ab initio optimization methods using DFT.[83] These calculations shed important insight into the activation barriers for chemical reactions between water molecules and silica clusters, although thermal effects are not included in these calculations.[83] Similar types of calculations have recently been performed by Konečný and Doren[84] and Ugliengo and coworkers.[85] With an eye toward dissolution of silica, Criscenti et al. studied the reaction of a silanol-containing cluster with a hydronium ion in the presence of four water molecules.[86] Ma et al.[87] have conducted ab initio MD simulations of water near different defects found in silica clusters and find that several waters are needed for the hydroxylation mechanisms they observe. More recently, Hamad and Bromley[88] have conducted longer thermal ab initio simulations to study the hydroxylation mechanisms of nonbridging oxygens (NBOs), oxygen atoms that have a single covalent bond to a silicon atom, in small silica clusters. These results suggest that the NBOs are a negatively charged, closed-shell species, whose hydroxylation is quite sensitive to the surface morphology. Du et al. have investigated the reaction of one or two water molecules with an amorphous silica surface using QM/MM techniques,[89] yielding information about the initial steps of

silica surface hydroxylation. Ab initio molecular dynamics have been used to study the reactions of water with the amorphous silica surface by Masini and Bernasconi[90] and Mischler et al.,[91] and the pK_a of silanol groups on crystalline silica surfaces by Leung et al.[92] Tielens et al.[93] initiated an AIMD simulation of a hydroxylated silica slab using a starting point from Garofalini's empirical potential models and studied the surface structure, making detailed comparisons with experiment. They calculated the deprotonation energy of silanol groups and the binding energy of individual water molecules. Trilocca and Cormack have reported AIMD studies of liquid water near the related water−bioglass interface,[94] and Leung et al. have reconstructed the bonding arrangement on crystalline silicate surfaces to mimic the amorphous surface.[92] To our knowledge, ab initio molecular dynamics of the amorphous silica−water interface, along the lines of what we provide in section 3, have not been reported.

We have performed AIMD simulations on a small hydrated silica slab in which one surface does not contain silanols and the other surface contains several silanols, one of which is dissociated. The relative wetting properties of silanol-rich and silanol-poor regions are confirmed, although the AIMD system was too small to quantitatively compare radial density distributions. We also compared AIMD and empirical results for a single orthosilicic acid molecule in water. Our potential was not designed to fit the properties of orthosilicic acid, but at least the comparison is much more direct because the size of the silicate system is not an issue. We find that the number of waters in the first and second solvent shells compares well for orthosilicic acid, although the radial densities of waters surrounding the silanol groups of orthosilicic acid are more structured in the AIMD simulations. A direct comparison between AIMD and empirical potential results is clouded by several factors. The empirical potential simulations of a silica surface encompass much more surface variability than the smaller, AIMD system. A further limit on our ability to benchmark our empirical potential with AIMD is the limitation on the accuracy of currently available density functionals and the numerical methods available for their implementation. The BLYP[95,96] and PBE[97] functionals, as normally implemented, lead to overstructuring of the water, lead to peaks in the radial distribution function of liquid water that are too high and narrow, and underestimate the diffusion constant.[98−100] The degree of overstructuring is sensitive to the details of the implementation and system size.[100] Lee and Tuckerman have shown that very accurate basis sets are needed to converge liquid state properties,[101,102] including the diffusion constant.[103] Exceptionally large charge-density cut-offs are needed to obtain a converged water density.[104]

In section 2, we describe the potential form that is used to model our interface between the dissociated silica surface, water, and salt. Within this section, we provide all the parameters of the model for the use of interested readers. We also compare the quality of our empirical potentials to the ab initio quantum chemistry cluster calculations that are used to generate our potentials. A comparison of some properties from the ab initio MD simulations on the smaller system to those predicted from our empirical model is reported in section 3. We also describe specific chemical events that occur during the first few picoseconds of our AIMD simulations. Finally, we end with a conclusion in section 4.

2. Development of a Model for Dissociated Amorphous Silica

2.1. Formulation of the Potential. Our goal is to model the amorphous silica/water interface using a computationally inexpensive model with sufficient realism to capture essential features of the electrical double layer, electrokinetic phenomena, and adsorbate binding. These phenomena require simulations that extend to large spatial and temporal scales. Models that can describe surface chemistry, either so-called dissociating potentials[44−46,53,105−107] or AIMD methods, are extremely valuable, but they are not sufficiently tractable for the large-scale calculations we envision. The chemical bond structure will be fixed in the model we propose, although the surface is not constrained to be rigid. For example, the equilibrium between undissociated and dissociated silanols will not be dynamic. For many purposes, the effects of the chemically diverse features of the silica surface can be captured by a distribution of various species on a surface of sufficient size, or a collection of different surface realizations.[108]

Like our empirical potential for the undissociated amorphous silica surface,[27−29] our model for the hydrated dissociated amorphous silica surface extends the BKS model for bulk silica[109] and SPC/E model for water[110] to describe the water−silica interface. Hence, the bulk silica and water regions are described by models that have been tested in a variety of physical situations. The BKS and SPC/E potentials succeed in describing physical properties of silicates, both crystalline and amorphous, and water, respectively, but they also have limitations. Among the limitations, especially for the BKS model, is unrealistically large partial charges, which are in place to mimic other physical effects. Concern about the large partial charges was a major motivation for us to compare with AIMD results. The simplicity of these models is both a virtue and limitation: a virtue in the sense that large-scale simulations are possible, but a limitation in that, even with the extensions put in place for surface species, the functional form cannot fit all the available data obtained in fragment ab initio calculations.

In keeping with the BKS model,[109] all silicon and oxygen atoms of the silica are assigned charges of +2.4 and −1.2. The BKS potential is a sum of pairwise Coulomb and Buckingham (exponential repulsion + r^{-6} attraction) interactions. To avoid excessive overall attraction between water and our undissociated silica surface, we found it necessary to distinguish between silanol-type and siloxane-type oxygens, for the short-range potentials.[27,28] As shown before, an acceptable fit to ab initio data could be achieved with these fixed charges[28] for the water−silanol clusters. Charge neutrality of the undissociated surface requires that the charge on hydrogen atoms be +0.6. In principle, it is possible to introduce silanol groups on the surface with different partial

charges from those used in the BKS potential. In the dissociated surface model, we have added a dissociated oxygen type, O^-, to include dissociated groups on the surface. The charge of the O^- group was required to have a value of -1.6 to maintain a net charge of -1 for each dissociated silanol generated in our simulations.

Without adjusting the charge on silicon atoms, the partial charges on silanol oxygen and hydrogen atoms could be adjusted away from their BKS values of -1.2 and $+0.6$, respectively, as long as their sum is kept at -0.6, required to maintain charge neutrality of the undissociated surface.[28] Further adjustment of the silanol group partial charges, or modification of the O^- charge, would require distinguishing surface silicon atoms with charges different from interior silicons. However, retaining the BKS charges for all atoms greatly simplifies the construction of the hydroxylated amorphous silica (section 3.2) because the atoms that will eventually anneal to surface positions after cleavage of pure silica are not known in advance. Furthermore, it should be noted that it is the sum of the Coulomb and short-range interactions (Buckingham or Lennard-Jones) that is ultimately fit to ab initio quantum chemistry calculations. While realistic partial charges are desirable, it is possible to compensate the unrealistic BKS partial charges with other parts of the complete interaction potential.

As mentioned above, our potential is designed to maintain a given bonded configuration, and not to predict making or breaking of chemical bonds. In some cases, the model has to be extended to prevent unintentional, and sometimes unphysical, bond formation driven by strong Coulomb interactions. Our potential for the undissociated surface included 3-body components that prevented the hydrogen atoms of silanols from binding to more than one oxygen atom.[28] We refer to these components as "blocking potentials". After the introduction of O^- groups, thermal simulations without the additional blocking potentials yielded species where the dissociated oxygen group (O^-) formed new bonds, either bonding to more than one silicon, mimicking a newly formed siloxane bond, or forming another (unphysical) species where the dissociated oxygen is divalently bonded to a silanol hydrogen and a silicon atom. We introduced two blocking potentials in addition to those used for the undissociated surface, given in eqs 1 and 2, which stabilized the chemical bond structure.

$$u_{\mathrm{SiO_DSi}}(r_{\mathrm{SiO_D}},r_{\mathrm{O_DSi'}}) = k\exp[-\rho^{-4}(r^4_{\mathrm{SiO_D}} + r^4_{\mathrm{O_DSi'}})] \quad (1)$$

$$u_{\mathrm{SiO_DH}}(r_{\mathrm{SiO_D}},r_{\mathrm{O_DH}}) = k\exp[-\rho^{-4}(r^4_{\mathrm{SiO_D}} + r^4_{\mathrm{O_DH}})] \quad (2)$$

Equation 1 is a 3-body interaction between the O^- of a dissociated silanol group (O_D) and two Si atoms (Si, Si′). Equation 2 is a similar potential involving a Si atom, O^-, and the hydrogen of a nearby silanol group. The values of k and ρ in eqs 1 and 2, which control the strength and range, respectively, of the 3-body blocking potentials are given in Table 1.

Because the BKS potential[109] consists of Buckingham potentials between the oxygen atoms, we also included three other Buckingham interaction potentials between each pair of O^- groups, a silanol oxygen and O^- group, and finally an O^- and siloxane oxygen. The total silica interaction potential including dissociated groups on the surface is now of the following form:

$$U = U_{\mathrm{pair}} + U_{\mathrm{3\text{-}body}} \quad (3)$$

$$U_{\mathrm{pair}} = \sum_{i=2}^{N}\sum_{j=1}^{N-1}\left(\frac{q_iq_j}{r_{ij}} + u_{ij}(r_{ij})\right) \quad (4)$$

While Buckingham potentials are often used to describe inorganic solids like silica, Lennard-Jones potentials

$$u_{\mathrm{LJ}}(r) = 4\varepsilon\left[\left(\frac{\sigma}{r}\right)^{12} - \left(\frac{\sigma}{r}\right)^{6}\right] \quad (5)$$

are commonly used for water, as for SPC/E, ions in water, and biomolecules. Because we need to interface with common force fields, we employed Lennard-Jones potentials, denoted by the symbol "LJ", for the salt, water, and silica interactions described below. The procedure used to fit the potentials and the quality of fits are described in the following section. The Lennard-Jones potential parameters are collected in Table 2.

In Table 3 are obtained the parameters A, ρ, and C_6 by fitting the ab initio data to a Buckingham potential of the form:

$$u_{\mathrm{B}}(r) = Ae^{-r/\rho} - \frac{C_6}{r^6} \quad (6)$$

The Buckingham potential as shown in eq 6 has an unphysical maximum at small r, and then plunges to $-\infty$ at even smaller r. It is thus standard to modify the Buckingham potential to eliminate the unphysical maximum and make it

Table 1. Interaction Parameters for the 3-Body Potentials, Eqs 1 and 2

atom triplet	k (eV)	ρ (Å)
$Si-O_D-Si$	1000.000	1.6
$Si-O_D-H$	100.000	1.6

Table 2. Pairwise Lennard-Jones Parameters, Eq 5

ion/atom pair	ε (eV)	σ (Å)
Na^+-O_W	0.005406	2.8760000
Cl^--Si	0.010823	3.8805759
Cl^--O_W	0.005406	3.7840000
Cl^--Na^+	0.004336	3.4920000
Cl^--H	0.006378	3.6253307

Table 3. Pairwise Buckingham Potential Parameters, Eq 6

atom pair	A (eV)	ρ (Å)	C_6 (eV Å^6)
$Si-O_D$	13 536.40	0.219247	128.344
O_D-O_D	1388.773	0.3623188	175.0000
O_D-H	5907.000	0.1254160	0.0000
O_D-O_W	6533.490	0.284692	336.7540
O_D-H_W	70.795	0.306200	0.0000
Na^+-O_H	5151.600	0.2725004	60.44529
Na^+-O_X	5151.600	0.2763590	60.00000
Na^+-O_D	40 286.40	0.2133588	70.40000

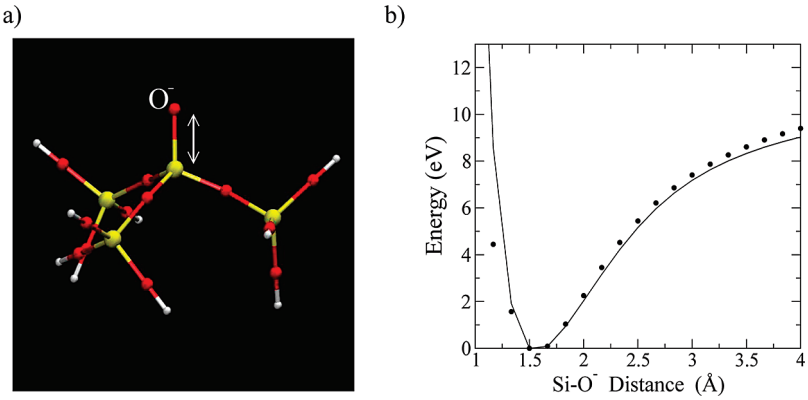

Figure 1. Fitted (solid line) versus ab initio energies (●) for (b) Si−O$^-$ stretch for fragment shown in (a).

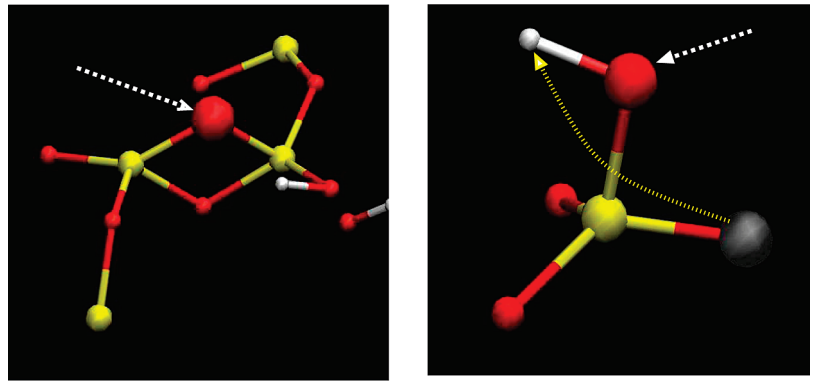

Figure 2. Left panel shows the formation of a two-membered ring involving a dissociated oxygen that is divalently bonded to two silicons. The dotted white arrow points in both cases to the dissociated oxygen involved in the interaction. In the right panel, the dotted yellow arrow shows the hydrogen that originates from one of the hydroxyl groups of a geminal silanol pair, which are attached to the same silicon atom.

smoothly repulsive at small r. Details of the small r patch are described in our previous work.[28]

For the convenience of those wishing to use the potentials, the final parameters forming the interaction potentials U_{pair} and $U_{\text{3-body}}$ for the extension of our undissociated surface are collected in Tables 1−3. Readers are referred to our previous work for the other interaction parameters that were unchanged in modeling the dissociated surface.[28,29] In the tables, the subscript "X" refers to oxygen types that are not connected to hydrogens but different from dissociated types (i.e., O$^-$), the subscript "D" refers to oxygen types that are dissociated, and the subscript "H" refers to oxygens that are part of silanol OH groups.

2.2. Parameter Adjustment To Match Ab Initio Data. Using fragments excised from a silica surface, ab initio quantum mechanical calculations were performed from which we fit our empirical potentials. As in our previous work,[28] the parameters of empirical potentials are adjusted to match ab initio data generated for coordinate grids. This section is devoted to describing the quality of the match between our empirical potentials and ab initio data. The Born−Oppenheimer energy surface was obtained using MP2 perturbation theory[111−115] to account for electron correlation. We use the 6-311++G** basis set, and all electronic structure calculations were performed using Gaussian 03.[116]

2.2.1. Dissociated Groups. The potential for the dissociated groups Si−O$^-$ consists of a single Si−O$^-$ Buckingham plus Coulomb interactions. The Si−O$^-$ distance in the fragment shown in Figure 1a is varied between 0.7 and 4.0 Å, and the resulting energies are used to fit the Buckingham potential form. The quality of the fit for the Si−O$^-$ stretch is shown in Figure 1b.

As indicated earlier, we found that thermal simulations without blocking potentials yielded configurations as seen in the left panel Figure 2 where an O$^-$ is divalently bonded to two silicons. We also found that the hydrogens of silanol oxygens can transfer to dissociated oxygens during the simulations as seen in the right panel of Figure 2. In this defect, the hydrogen on the dissociated oxygen group originated via the deprotonation of the silanol oxygen shown in translucent red. Our model is not intended to capture realistic deprotonation and protonation of oxygen species on the surface. To prevent new chemical structures from forming on the surface, we inserted 3-body blocking potentials as described in eqs 1 and 2. These were not fit to ab initio data. Instead, the parameters were adjusted by trial and error until these defects no longer occurred. Our potential form also includes the BKS Buckingham potential between the dissociated oxygen type and all other oxygens and silicon atoms of the silica surface to ensure that the surface bond structure remains intact.

2.2.2. Water-Dissociated Silica Interactions. The water-dissociated silica potentials were fit using a path of approach for a water molecule near a dissociated group shown in the left panel of Figure 3. The water-dissociated oxygen separation was varied from 1.8 to approximately 13 Å to obtain a

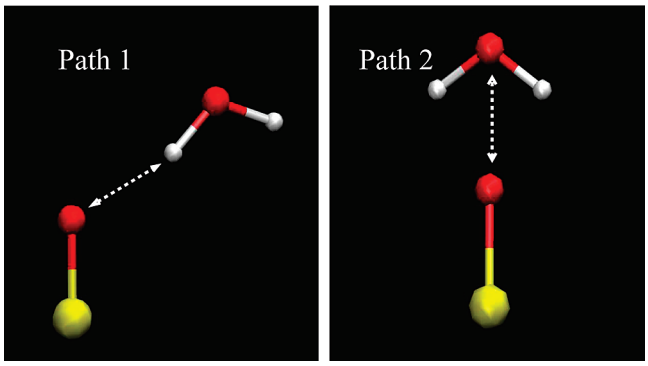

Figure 3. Paths of approach for water near a dissociated silanol.

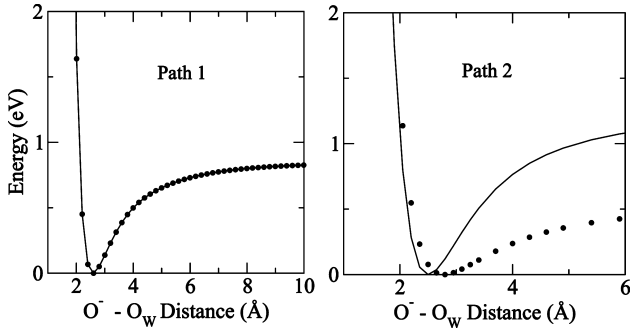

Figure 4. Fitted (solid line) versus ab initio (filled symbols) energies for the paths of approach shown in Figure 3. On the left are path 1 energies, and on the right path 2 energies.

comprehensive sweep of the potential energy surface. The water geometry was fixed to that of the SPC/E model[110] and was not allowed to relax as it approached the dissociated silanol. This scheme is similar to our design of a potential between water and undissociated silanols, for which the reader is referred to our previous work.[27,28]

In most common water−water and water−ion potentials, only the water oxygen carries a non-Coulombic interaction, like a Lennard-Jones potential. The potential surface for these common water potentials contains basins where the potential diverges to $-\infty$ when a hydrogen is superimposed on an oxygen. These unphysical regions are never discovered in simulations. However, the dissociated silanol oxygen carries a large negative charge, and the attractive Coulomb infinity was discovered in preliminary simulations. We found it necessary to include an exponential repulsive Buckingham between the dissociated oxygen and water hydrogen (O_D-H_W potential).

To test the transferability of our water-dissociated silica potential to another path of approach, a water molecule was brought toward a dissociated oxygen shown in the right panel of Figure 3. Ab initio calculations indicate that path 1 (Figure 3) is the more favorable path for approach of a water to a dissociated silanol. We were not successful in reproducing this feature in our empirical potential using the available flexibility in the Buckingham + Coulomb form of our potential, together with the many constraints on partial charges (BKS charges for silica Si and O, SPC/E charges for H_W and O_W). Figure 4 shows all the ab initio energies for the two paths of approach, and the predictions of our

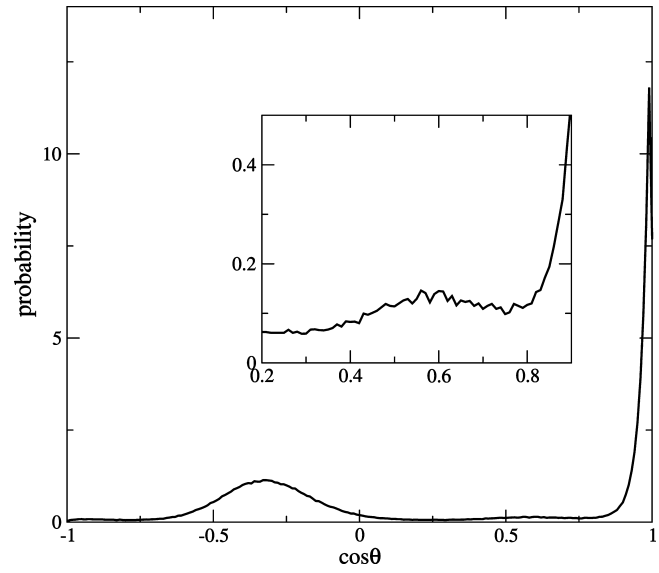

Figure 5. Orientational distribution of water near dissociated oxygens. The distribution is given for the dot product between unit vectors linking water oxygens to a dissociated surface oxygen (O_W-O_D) within a distance of 3.5 Å, and vectors along each of the two hydrogen bonds. The data confirm that in the thermal simulations, path 1 (Figure 3) is favored over path 2. The inset shows a small peak near the cosine of one-half the tetrahedral angle, the angle of the bifurcated structure of path 2.

empirical potential for each of these paths. Rather than "split the difference", we chose to fit the ab initio results along path 1 because preliminary simulations indicated that the binding geometry of path 1 was preferred, even when the most stable orientation of an isolated water was the bifurcated structure of path 2. This tendency is confirmed for the final form of the potential. Figure 5 shows the distribution of the angle between the vectors O_W-O_D and O_W-H_W for waters within 3.5 Å of each O^- group on the dissociated surface. These results show that in the thermalized simulations the cosine of the angle of one of the two water hydrogens is close to 1, and hence path 1 is the most likely orientation on the surface despite the fact that our empirical potential predicts a higher binding energy for a single water molecule along path 2. In Figure 5, there is a second peak near $\cos\theta = -1/3$ for the hydrogen not hydrogen bonding to the dissociated oxygen. The inset in Figure 5 reveals a very small peak corresponding to the bifurcated structure.

2.2.3. Na^+ and Cl^- Silica and Water Interactions. Initial simulations indicated that the Na^+ ions can strongly interact not only with dissociated silanols, but also silanol and siloxane oxygens. For this reason, we selected fragments from our simulations with and without a dissociated silanol, where a Na^+ ion interacts with all species to generate empirical potentials for these interactions.

Shown in Figure 6 are the three fragments that were used for the ab initio calculations. The first fragment consists of a sodium ion interacting with a single dissociated oxygen and siloxane oxygens. The second fragment consists of a sodium ion interacting with the silanol and siloxane oxygens, while the third fragment consists of a sodium ion interacting with all three species of oxygens. The free parameters of

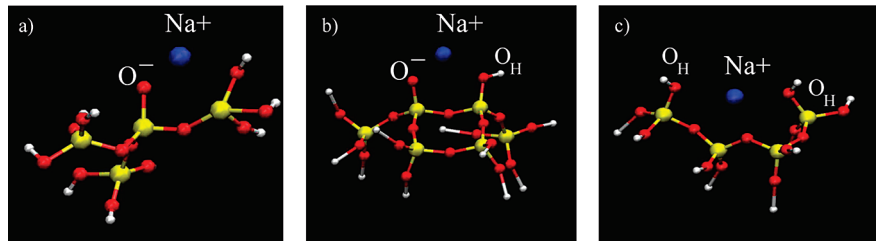

Figure 6. The three fragments used for silica−sodium interactions labeled (a) with a single O_D, (b) with a single O_D and silanol OH, and (c) with three silanol OH's. Unlabeled red spheres correspond to siloxane oxygens in our empirical potential. The blue sphere is the sodium ion.

Table 4. Fitted and Ab Initio Binding Energies for Silica−Na^+ Fragments

fragment	ab initio (eV)	empirical (eV)
frag 1	−6.44	−5.59
frag 2	−6.85	−7.35
frag 3	−3.05	−2.98

the sodium−oxygen Buckingham potential given in Table 3 were adjusted to match the ab initio binding energies.

For the fragments with a dissociated oxygen, it was not possible to generate a full potential energy surface representing the approach of a Na^+ ion to a surface fragment using ground-state ab initio methods. Without solvent, the ground state of this system at large separations is a neutral sodium atom and neutral fragment. The ground state becomes ionic in character as the sodium approaches the fragment. Hence, we relied on the binding energy to fix the non-Coulombic interaction parameters between the Na^+ ion and silica, the partial charges being constrained to the BKS values. The binding energy was calculated by separately calculating the energy of the ion−fragment complex, and then the energies of the isolated ion and fragment.

$$\Delta E_{\text{bind}} = E(\text{fragment/Na}^+) - E(\text{fragment}) - E(\text{Na}^+) \tag{7}$$

The comparison of the empirical and ab initio binding energies of a Na^+ ion to the three fragments shown in Figure 6 are reported in Table 4. The Si−O bond length and the position of the sodium ion were initially optimized with an ab initio calculation for the first fragment shown in Figure 6a. The Si−O bond length used in the other two fragments was very close to the optimized bond length obtained for the first fragment.

Chloride ions are repelled from a negatively charged silica surface, and, as compared to sodium, chloride ions will have considerably weaker interactions with the silica surface. Hence, the interactions between the chloride ions and the silica surface were calibrated without further quantum chemical calculations using available potentials in the GROMOS96 force field.[117] Our preliminary simulations also indicated that the Cl^- ions quickly explore the Coulomb infinity at the positively charged silicon and silanol hydrogen atoms. For this reason, short-range LJ potentials were inserted between these species. These potentials were derived using combining rules with potentials from the GROMOS96 force field. The interaction parameters between the sodium and chloride ions and water were obtained from previous work by Dang.[118] The parameters used in our simulations are shown in Table 2.

3. Comparison of Ab Initio and Empirical Results

3.1. Simulation Methods. In this section, we describe the evaluation of our empirical potential using ab initio MD simulations on a smaller hydrated slab system. Because of computational feasibility, AIMD simulations were limited to rather small systems. The starting configuration for the AIMD simulations was generated by annealing a bulk crystalline silica tridymite structure with no free surfaces measuring 10.13 Å × 17.55 Å × 8.275 Å, and consisting of 32 silicon atoms and 64 oxygen atoms using the BKS potential[109] with dispersion interactions truncated to one-half of the shortest side of the box. The protocol that was used to generate amorphous silica from the starting material was adopted from cycle I−IV of Huff and co-workers,[119] as in our previous work. We cleaved the surface by opening a gap in the z-dimension, followed by annealing for 5 ps at 300 K. This small surface yielded one two-membered ring on one surface and no structural features on the other surface that would lead to silanol groups. The two-membered ring was opened with the addition of water to form two nearby silanol groups in a process described below in section 3.2, initially yielding a total of 2 silanols on one of the surfaces and no silanols on the other. After hydroxylation, a total of 71 waters were added to the system. This hydrated silica slab was then used as input for the ab initio MD simulations. Further reaction of water with the surface during the ab initio MD simulations led to the appearance of more silanol groups on the side that already contained silanols, and none on the other side of the slab. This is appealing because it furnished a means to test our findings[28] that silanol groups make the silica surface hydrophilic, while surfaces depleted in silanols are relatively hydrophobic.[78] Unfortunately, we were unsuccessful in conducting a classical simulation of systems of the hydroxylated surface using our empirical potential due to technical limitations implementing 3-body interactions in the DLPOLY package for a small system size. For this reason, we could not use a starting configuration for the ab initio MD simulations obtained by first equilibrating with our empirical potential, or compare data for AIMD and empirical simulations of exactly the same system. We emphasize that the 3-body interactions were omitted only for the small system size that is used to generate a starting configuration for the ab initio MD simulations. The 3-body

Table 5. Summary of Systems Simulated in This Work Using Both Our Empirical Model and the Ab Initio MD Method[a]

system	method	simulation length	cell dimensions
large dissociated silica slab	empirical	9 ns	32.83 × 32.84 × 127.59 Å^3
small silica slab (initial configuration for AIMD)	empirical	145 ps	10.13 × 17.55 × 8.275 Å^3
small silica slab + excess proton	AIMD (DZVP)	22 ps	8.837 × 15.309 × 27.219 Å^3
small silica slab + Na^+	AIMD (DZVP)	15 ps	8.837 × 15.309 × 27.219 Å^3
orthosilicic acid	empirical	2 ns	12.75 × 12.75 × 12.75 Å^3
orthosilicic acid	AIMD (DZVP)	20 ps	12.75 × 12.75 × 12.75 Å^3
orthosilicic acid	AIMD (TZV2P)	15 ps	12.75 × 12.75 × 12.75 Å^3

[a] The 9 ns empirical model simulation was used to obtain the results presented in section 3. The small, 145 ps empirical simulation provided the starting configuration for the AIMD simulations of a silica slab.

interactions were implemented for the larger systems that are used in our production runs to compare the empirical and ab initio MD results.

The AIMD simulations were conducted using Quickstep, which is part of the CP2K package.[120,121] In these calculations, ab initio Born−Oppenheimer molecular dynamics is used for propagation of the classical nuclei. The electronic orbitals are converged to the Born−Oppenheimer surface at every step in the molecular dynamics simulation. The wave function was optimized using an orbital transformation method[122] in conjunction with the DIIS scheme,[123,124] as described in ref 121. The convergence criterion for optimization of the wave function was set to 10^{-6}. Using the Gaussian and plane waves (GPW) method, the wave function was expanded in the Gaussian DZVP basis set. While a triple-ζ basis set was not feasible for the silica slab, simulations using the larger TZV2P basis set were used to check convergence of our radial distribution functions with respect to basis set size for orthosilicic acid in water, as reported below. An auxiliary basis set of plane waves was used to expand the electron density up to a plane wave cutoff of 300 Ry. We used the Becke−Lee−Yang−Parr gradient correction[95,96] to the local density approximation and Goddecker−Tetter−Hutter (GTH) pseudopotentials.[125] A time step of 0.5 fs was used in all ab initio simulations. During the first 3 ps of the simulation, we observe several chemical processes that occur on the surface. These chemical processes will be documented in detail later. At this stage, reaction with water adds 3 silanols to the surface that already contained 2 silanols. Exchange of hydrogen and oxygen atoms between the water molecules and atoms on the silica surface results in the formation of an extra proton that, during the length of our simulations, fluctuates between two Eigen structures and samples a Zundel complex during the fluctuations. The presence of the excess proton in the solvent near the surface during the course of the simulation suggests that the silica slab is negatively charged, which is confirmed below. The simulation with the proton in the bulk was then run for a total of approximately 22 ps. For data analysis, the first 6 ps of this simulation was treated as equilibration. An additional simulation was begun from a configuration chosen from the first 3 ps of this simulation, where the proton was replaced by a Na^+ ion. This simulation was run for a total of approximately 15 ps. For the data analysis, the first 4.5 ps of the run with Na^+ was treated as equilibration. All the AIMD simulations described were conducted within the NVE ensemble.

We also conducted AIMD simulations of orthosilicic acid using the DZVP and TZV2P basis sets. These simulations consist of a single orthosilicic acid molecule ($Si(OH)_4$) surrounded by 66 water molecules in a box of side length 12.75 Å. Using the same methodology described above, AIMD simulations of length 20 ps were conducted using the DZVP basis set and 15 ps using the TZV2P basis set. Simulations of this system were also performed using our empirical model. All the simulations conducted with our empirical model and DFT ab initio method are summarized in Table 5.

3.2. Construction of a Dissociated Silica Surface. In our previous work,[28] we described the method used to generate a hydroxylated silica surface. We will briefly review some of those procedures in this section. The starting configuration begins with crystalline tridymite with no free surfaces. The amorphous silica slab is then generated using a protocol adopted from cycle I−IV of Huff and co-workers.[119] The slab is cleaved by opening a gap in the z dimension followed by annealing for a limited time at 300 K. The silica surface consists of various species such as two-membered (2M) rings, nonbridging oxygens (NBOs), and three coordinated silicons. In Table 4 of our earlier work,[28] we showed that the length of annealing time in the simulations controls the population of these species on the silica surface and consequently the silanol density of the silica surface. Thus, the concentration of silanols on the surface can be controlled in a systematic way to reproduce reported experimental values of the silanol density.[1,126] The 2M rings were manually converted into a pair of vicinal silanols, that is, two close by silanols, as seen below:

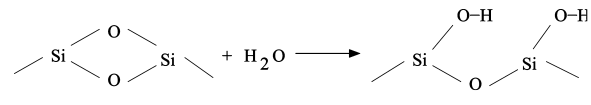

while the NBOs were transformed into geminal silanols:

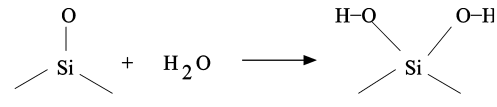

which are attached to the same silicon atom. These procedures follow likely hydroxylation reactions identified by previous ab initio calculations[90,91,127,128] as described in our earlier work.[28] The detailed structure of the aqueous silica surface, its mechanism of hydroxylation, and the distribution of isolated, vicinal, and geminal silanols have not yet been conclusively established theoretically or experimentally, and certainly more work is needed in this area.

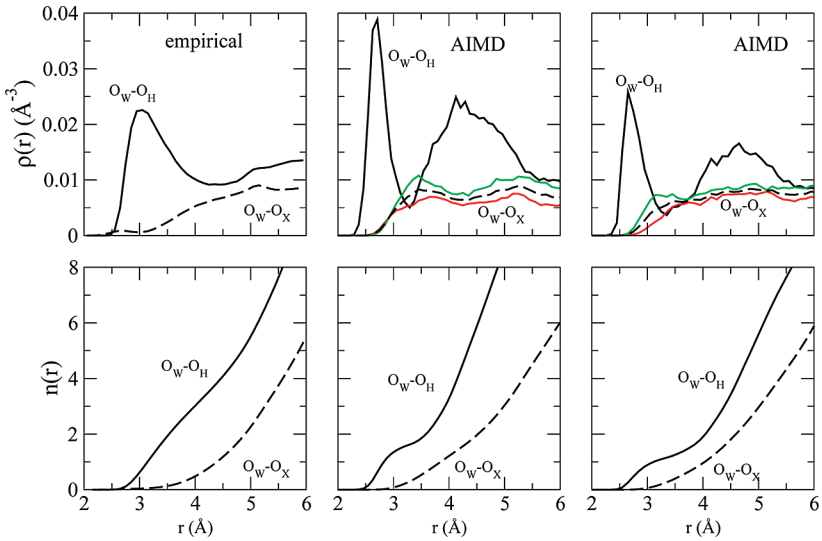

Figure 7. Radial density of water (top row), and cumulative number of neighboring waters (bottom row) near silanol (solid line) and siloxanes (thick dashed lines) for the empirical model shown in left panel, AIMD simulation with proton in middle panel, and AIMD simulation with Na^+ shown in right panel. The green and red thick lines are radial densities near siloxanes in only hydrophilic and only hydrophobic regions, respectively.

Once the hydroxylated surface is formed, silanols on the surface need to be selected for deprotonation to form O^- groups. Because of the lack of any experimental or theoretical insight, the silanols are deprotonated in a random fashion except that we never deprotonate both hydroxyl groups of geminal silanols because we expect that charge repulsion will make doubly dissociated geminals a high energy species. For the simulations reported here using our empirical model, 18 dissociated sites, 9 on each surface of the silica slab, are chosen so that they are separated by at least 6 Å. Our empirical simulations for the dissociated surface consist of a box measuring 32.83 Å × 32.84 Å × 127.59 Å. Along the box height of 127.59 Å, water occupies approximately 92 Å, and the silica slab fills the remainder. The charge density of the surface was 0.835 e nm^{-2}.

3.3. Radial Densities Near Silanol Groups of Silica and Orthosilicic Acid. Shown in Figure 7 is a comparison of the radial distribution functions for water near the silanol oxygens and siloxanes from our empirical model, and for the ab initio simulations for the two systems described above. We note that the striking difference in water density near silanol and siloxane oxygens, originally noted in our study of the undissociated surface,[28] is confirmed by AIMD. Previously, we had reported[28] that our empirical model did not perform favorably in reproducing the paths of approach of a single water molecule to a siloxane group as compared to ab initio results. This discrepancy does not appear to directly affect the hydrophobic/hydrophilic property of the surface. Water is depleted near siloxanes regardless of the proximity of silanol groups. It occurs on both sides of the AIMD slab, the side with no silanols and the side with 5 silanol groups (red and green curves in Figure 7).

The comparison between empirical and AIMD radial water densities in Figure 7 shows under-structuring by our empirical potential as compared to AIMD in the form of lower and wider density peaks. Also, the radial distribution function (RDF) for the water oxygen−silanol oxygen peaks at about 3.0 Å in our empirical model, but is peaked at about 2.7 Å in the ab initio simulations. Studies of orthosilicic acid reported below confirm that part of this trend can be attributed to the empirical potential parameters, which tend to under-structure water near silanol groups. However, very limited sampling of silanol group environments in the AIMD runs also contributes significantly to the difference between AIMD and empirical results in Figure 7. As noted earlier, it was not possible to carry out empirical and AIMD simulations on exactly the same system. The empirical potential simulations were performed on a much larger sample. The surface area of the slab used in the empirical potential simulations is approximately 8 times that used in our AIMD simulations. Thus, the empirical potential simulations encompass a much larger range of silanol environments. The variety of local environments is illustrated by radial density plots for water near four individual silanol groups in our empirical potential simulations shown in Figure 8. A buried silanol group is found in the left-most plot, and the cumulative population plot beneath it shows that relatively few waters are surrounding it. All four examples exhibit a sharper first peak than the overall average for the empirical potential surface in Figure 7, where such features are washed out. The right-most plot in Figure 8 shows a silanol group with abundant exposure to water and a pronounced minimum between the first and second peaks. In contrast to the diversity encompassed by the empirical simulation, the environments for the five silanol groups in the ab initio simulations were relatively similar, and individual radial water densities near individual silanol groups for the AIMD runs did not show strong variation. To obtain a quantitative comparison of the radial distribution functions, larger AIMD system sizes over multiple realizations that have surface morphology similar to that used in our larger empirical model would be required.

In the left and right panels of Figure 9, we compare the radial densities of sodium ions and water about dissociated groups and the radial density of water about sodium ions from our empirical model and AIMD simulations, respectively. As mentioned before, the AIMD simulations consist

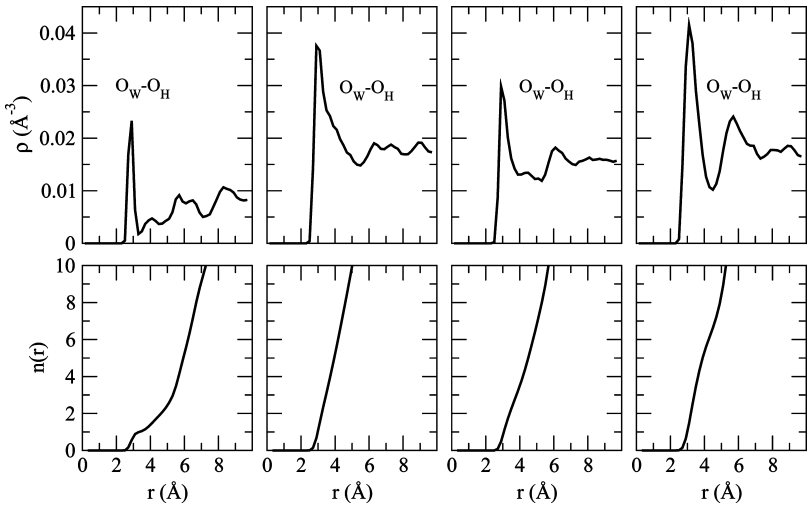

Figure 8. Radial density of water (top row), and cumulative number of neighboring waters (bottom row) near four individual silanol groups from empirical potential simulations.

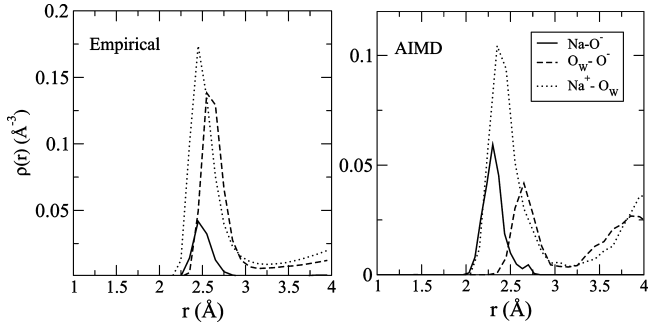

Figure 9. Radial density of Na^+ ions near O^- groups (solid thick line), O_W near O^- groups (solid dashed lines), and Na^+ near O_W (solid dotted line) for our empirical model in the left panel and AIMD simulations in the right panel.

of only a single sodium ion, while the empirical model simulations are averaged over many sodium ions and dissociated O^- groups. As for silanol groups (see discussion of Figure 7), we cannot make a direct comparison of O^- groups averaged over the entire empirical potential surfaces with a single O^- group in the AIMD simulation. With these caveats, a comparison of the positions of the maxima of the various densities suggests that our empirical model for the dissociated surface at least does not contradict the AIMD results. The O^-—Na^+ density peaks at about 2.3 Å for the single dissociated oxygen in the AIMD simulations and 2.45 Å in our empirical model over 18 dissociated oxygens. The O_W—O^- density peaks at about 2.65 Å in the AIMD simulations and 2.6 Å in the empirical model, and finally the Na^+—O_W density peaks at about 2.4 Å in the AIMD and at 2.45 Å in our empirical model. The empirical model qualitatively reproduces the trend observed in the AIMD simulations of a larger first peak position in the O^-—O_W radial density as compared to the first peak positions in the O^-—Na^+ and Na^+—O_W densities.

The radial densities of the water oxygens and atoms on orthosilicic acid are shown in Figure 10. The radial densities show good agreement between the DZVP and TZV2P basis

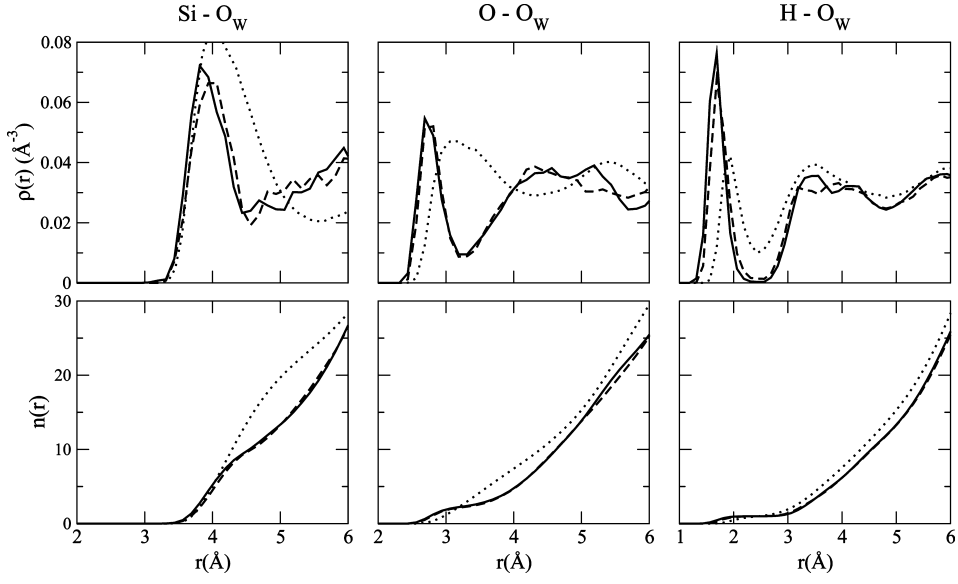

Figure 10. Radial density of water (top row) and cumulative number of neighboring waters (bottom row) near silicon, oxygen, and hydrogen atoms of orthosilicic acid shown for DZVP (solid black), TZVP (solid dashed), and empirical model (solid dotted).

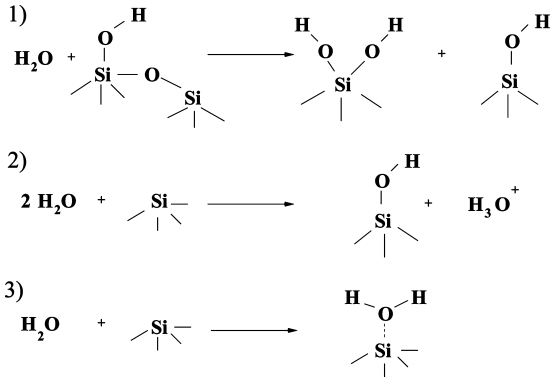

Figure 11. Three different chemical processes that occur within the first 3 ps of our AIMD simulations are labeled 1−3. The first shows the conversion of an isolated silanol (silicon atom with a single hydroxyl group) to a geminal silanol and another isolated silanol. The second shows the formation of an isolated silanol and a hydronium ion, and the third shows a single water molecule sticking to an exposed silicon atom on our hydrophobic surface.

sets, suggesting that the radial densities in Figure 7 that confirm the hydrophilic (hydrophobic) property of silanols (siloxanes) are at the very least qualitatively converged with respect to the basis set. Convergence with respect to the charge density cutoff was not explored.[104] We find that our empirical model, which was not designed to model orthosilicic acid, under-structures the water near the orthosilicic acid. However, the cumulative neighbor populations shown in the bottom row of Figure 10 demonstrate that the number of waters near orthosilicic acid matches well between AIMD and our empirical model.

3.4. Description of Surface Chemistry in AIMD Simulations. We observed interesting chemical processes occurring on the surface within the first 3 ps after a freshly cleaved silica surface was exposed to water in ab initio simulations. This resulted in the formation of three more silanol groups on one surface. Some of these important events will be reviewed in this section. These results should be viewed as preliminary information on processes that deserve much further study. It should be noted that the starting configuration for the AIMD simulations was not pre-equilibrated using our empirical potential and hence represents a high energy starting configuration that is subject to significant surface relaxation. Further work is needed to show how sensitive the occurrence of these chemical events is to larger system sizes, and different initial surface morphologies that may arise from annealing and equilibration protocols using our empirical model.

The schematic shown in Figure 11 illustrates three separate process that occur on our surface. The first process shows the conversion of an isolated silanol to a geminal silanol and another isolated silanol, resulting in the addition of two more silanols to the surface. The intermediate steps are seen more clearly in Figure 12. As a water molecule binds strongly to the silicon atom of the isolated silanol, one of the Si−O bonds associated with the silicon atom lengthens, resulting in a nonbridging oxygen (Figure 12i). At the same time, the water molecule splits, donating an OH group to the silicon, transiently forming a hydronium ion H_3O^+ (Figure 12ii). The proton that forms the transient hydronium is then recaptured by the newly formed silanol. Simultaneously, the hydrogen that was originally added as part of the OH group to the silicon is transferred to the nonbridging oxygen (Figure 12iii). The resulting product is a geminal silanol and an isolated silanol (Figure 12iv). The role of the formation of transient hydronium ions during the chemisorption of small numbers of waters onto the silica surface has previously been observed by Du et al. in QM/MM simulations, by Mahadevan and Garofalini using a dissociating potential model,[48,50] and, for large silica clusters, by Ma et al. with ab initio MD simulations.[87]

Snapshots from the second hydroxylation scheme of Figure 11 are shown in Figure 13. A two-coordinate silicon is transformed into an isolated silanol along with the transfer of a proton to the water. Ma and co-workers,[87] who have also conducted ab initio MD simulations of water near silica clusters, found that the two-coordinate silicons in their simulations were highly unreactive with water. In our simulations, we observe that as the water molecule strongly binds to the under-coordinated silicon, the OH group of the water is transferred to the silicon, and the proton is transferred to the surrounding water forming a hydronium ion H_3O^+. During the transfer of the OH group from the water to the silicon, one of the Si−O bond lengths associated with the silicon increases by approximately 0.2 Å. This process involves charge separation between the slab and the solvent, as illustrated by the charges in Table 6 obtained using the DDAP[129] charge partitioning method from 192 configurations

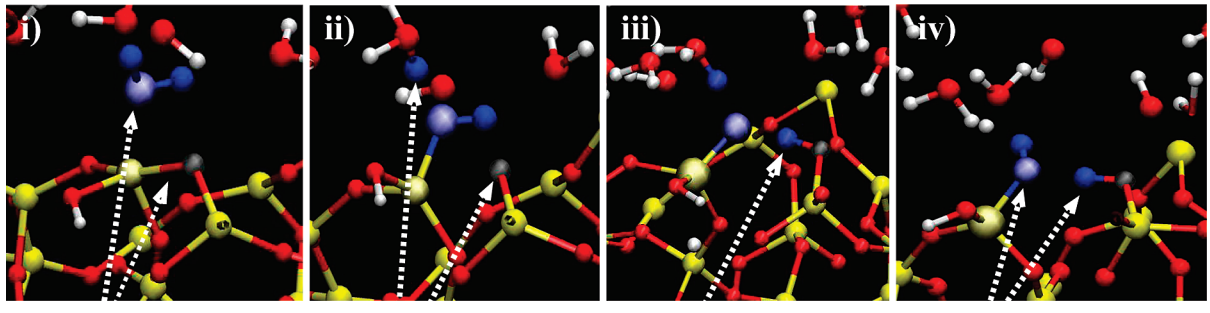

Figure 12. Steps in the formation of a geminal and isolated silanol from an initial single silanol, process (1) in Figure 11. The atoms of the water molecule that reacts with the surface are shown in blue in all four frames. (i) Arrows point to water that attacks silicon atom and Si−O bond that begins to break. (ii) Arrows point to the non bridging oxygen formed after the Si−O bond breaks and the hydronium ion transiently formed. (iii) Arrow points to the proton transferred from the newly formed silanol to the NBO. (iv) Final products are a geminal and a single silanol.

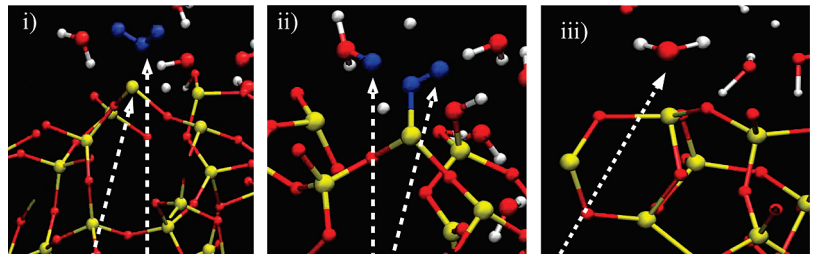

Figure 13. The left and middle frames illustrate steps in the formation of an isolated silanol from an under-coordinated silicon, scheme 2 of Figure 11. The atoms of the water molecule that reacts with the surface are shown in blue in these frames. (i) Water attacks an undercoordinated silicon atom. (ii) An OH group is added to silicon and hydronium ion is formed. (iii) The frame on the right shows a water molecule on the hydrophobic surface that binds to an exposed silicon atom without further reaction during the length of the AIMD simulation.

Table 6. Average Charges of Species in AIMD Simulations[a]

species	slab + excess proton	slab + Na^+
slab	−0.923	−0.807
O (silanols)	−0.659	−0.690
O (siloxanes, hydrophilic side)	−0.830	−0.792
O (siloxanes, hydrophobic side)	−0.782	−0.794
NBO	−0.832	−0.904

[a] Charges were obtained according to the DDAP[129] charge partitioning scheme, which is based on the electron density.

after an excess proton is transferred to the solvent. The silica slab carries close to a full electron charge (− 0.923), and the solvent carries a corresponding positive charge. All the oxygens of the silica slab have a charge close to −0.8, including NBOs. After a proton was transferred to the solvent and the surface was stabilized, we could identify a buried NBO within a cleft on the surface, which was solvated by a single water molecule. This could be considered as the location of the excess charge on the silica slab.

The initial configuration for the AIMD simulation with the Na^+ was constructed by replacing a proton from the newly formed H_3O^+ (Figure 13ii) with a Na^+. The newly formed silanol (Figure 13ii) was deprotonated to form a nonbridging oxygen (NBO), and the proton was transferred to a nearby siloxane oxygen, which was converted thereafter into a silanol. The charge partitioning analysis was conducted for 192 configurations sampled from our simulations with the Na^+. The magnitude of the charges is shown in Table 6. The average charge of the Na^+ in our simulations is +0.726, indicating that a significant amount of the positive charge has leaked to its surroundings. Furthermore, the data also suggest that a significant proportion of the formal −1 charge of a singly dissociated silica surface leaks out on to its environment. Charge transfer between solvated ions and solvent has already been reported in several systems. Klein and co-workers[130] conducted ab initio simulations of a zwitterionic peptide, halide anions, and alkali cations in water. They observed a substantial amount of charge transfer between the carboxylate terminus and the solvent (0.1*e*). Similar values were also found for K^+ and Na^+ ions. Chloride and bromine anions were found to transfer more electronic charge (0.26*e*) onto the surrounding solvent.

It is interesting that the charges of the oxygens of hydrophilic silanol groups are less than the oxygen from hydrophobic siloxane bonds in Table 6, once again confirming that hydrogen-bonding interactions are not purely electrostatic. The magnitude of the density-derived charges from the AIMD simulations, especially for silica atoms that follow the BKS model, is less than the charges used in our model. However, these differences do not preclude qualitative agreement between the empirical and AIMD predictions of the hydrophobic/hydrophilic property of the silica surface. Future work in the development and improvement of empirical models for amorphous silica may require adjustment of the charges in the empirical potential, guided by data shown in Table 6.

Finally, we find that the oxygen of a single water molecule interacts intimately with a 4-coordinated silicon atom throughout the length of our simulation on the hydrophobic side of the silica surface (third scheme of Figure 11 and right panel of Figure 13). The $Si-O_W$ distance for this water molecule fluctuates between 1.8 and 2.0 Å. Although the silicon atom is quite exposed to solvent, we do not observe any chemistry occurring at this site within the time scales of the simulations conducted. Perhaps longer simulations would lead to a hydroxylation event.

4. Conclusion

In contact with aqueous solution with pH greater than ∼3, the silica surface is negatively charged because a fraction of the silanol groups are dissociated and an electrical double layer is present.[1] In this work, we extended our empirical model for the undissociated surface. The silica surface in this model is flexible, so it can be used to model heat transport in nanoscale devices. The extended model now includes deprotonated silanol groups, and specifies water and sodium and chloride ion interactions with the surface. We employed the same strategy that was used in the previous model for the undissociated surface,[27,28] fitting the parameters of our empirical potential to accurate ab initio cluster calculations.

We have made comparisons with experimental quantities, such as the heat of immersion, where measurements are available.[28] Otherwise, we have relied on comparisons with quantum chemical and ab initio molecular dynamics results. We used well-calibrated and widely used models, BKS[109] and SPC/E,[110] to describe bulk silica and water, respectively, away from the interface. However, these models employ somewhat unrealistic partial charges to mimic other physical

interactions. Therefore, the benchmarking against quantum chemical and AIMD data is essential. We have confirmed a key prediction of our empirical potential, the striking difference in water density near silanol and siloxane groups. Despite the fact that the partial charges of the empirical model, especially the BKS parameters, are larger than those predicted by electron density calculations, the data for orthosilicic acid suggest that, if anything, our silica surface slightly under-structures nearby water. Populations of neighboring water near the surface are in good agreement with AIMD results. The evident under-structuring of our empirical potential as compared to AIMD may be, in part, attributed to the tendency of the BLYP density functional to over-structure hydrogen-bonding fluids, as discussed in the Introduction. The hydroxylation of a freshly cleaved silica surface is poorly understood, as is the distribution of various chemical groups on the surface.[2] Further tests of the convergence of AIMD methodologies to this system are needed before quantitative benchmarks can be established. We have provided an account of the reactions that occur in our AIMD simulations as water comes in contact with silica, and general agreement is found with previous theoretical studies of water chemisorption using small numbers of water near silica.[48,87,89] However, given the experimental difficulties in disentangling the complex structure of the silica surface, this is an area where extensive further AIMD investigations are needed.

In this work, we have compared the distribution of water near silanol groups on a smaller amorphous silica slab using ab initio MD simulations, and using our empirical potential. We have also compared the radial density of water near orthosilicic acid. For the slab systems, the surface heterogeneity of the larger system simulations performed with our empirical model complicates the comparison with the smaller ab initio MD simulations (see Figures 7 and 8 and the corresponding discussion). When our model is applied to simulating orthosilicic acid, we find that it results in the understructuring of water near the silanols. At this point, we cannot conclusively determine whether this behavior is an artifact of the density functional used in the ab initio MD simulations or whether our empirical model under-structures water near the silanols, or a combination of both.

An interface between water and amorphous silica is found in many applications, ranging from chromatography to novel nanofluidic devices. Our potential model is designed to enable atomistic device simulations at large length and time scales, which is desirable for several reasons. Large length scales are needed to go beyond straight channels and model features like nozzles or bends. Long time scales are needed to model fluid flow. Typical flow velocities are many orders of magnitude smaller than a typical thermal velocity, $(k_BT/m)^{1/2}$, where m is the molecular mass. As a result, flow velocities in nonequilibrium simulations are obtained by averaging over much larger numbers. The strategy in such simulations is to induce unrealistically large flow velocities to improve signal-to-noise, yet to keep the flow velocity below the point where nonlinear effects arise. The largest tolerable flow rates are on the order of 10% of a thermal velocity,[131] which means that extensive averaging is needed. Use of equilibrium simulations to evaluate Green−Kubo expressions has recently been advocated as an efficient alternative to nonequilibrium simulations for the calculations of transport coefficient[132,133] and flow profiles.[134,135] In either case, these calculations are demanding, underscoring the need for interaction models for the amorphous silica−water interface that combine computational efficiency with an acceptable level of realism, which is addressed in this work.

Acknowledgment. This material is based upon work supported by the National Science Foundation under Grant No. EEC-0914790. The calculations reported here were made possible by a grant of resources from the Ohio Supercomputer Center.

References

(1) Iler, R. K. *The Chemistry of Silica*; Wiley: New York, 1979.

(2) Legrand, A. P., Ed. *The Surface Properties of Silicas*; Wiley: New York, 1998.

(3) Fubini, B. In *The Surface Properties of Silicas*; Legrand, A. P., Ed.; Wiley: New York, 1998; pp 415−464.

(4) Unger, K. K. *Porous Silica, Its Properties and Use as Support in Column Liquid Chromatography*; Elsevier: New York, 1979.

(5) Jennings, W. *Comparisons of Fused Silica and Other Glass Columns in Gas Chromatography*; Alfred Huthig Verlag: New York, 1981.

(6) Towner, P. In *Essential Molecular Biology*; Brown, T. A., Ed.; Oxford: London, 2000; Vol. 1, Chapter 3, pp 55−67.

(7) Nanassy, O. Z.; Haydock, P. V.; Reed, M. W. *Anal. Biochem.* **2007**, *365*, 240–245.

(8) Cady, N. C.; Stelick, S.; Batt, C. A. *Biosens. Bioelectron.* **2003**, *19*, 59–66.

(9) Rech, I.; Cova, S.; Restelli, A.; Ghioni, M.; Chiari, M.; Cretich, M. *Electrophoresis* **2006**, *27*, 3797–3804.

(10) Liang, X.; Morton, K. J.; Austin, R. H.; Chou, S. Y. *Nano Lett.* **2007**, *7*, 3774–3780.

(11) Zhang, B.; Wood, M.; Lee, H. *Anal. Chem.* **2009**, *81*, 5541–5548.

(12) Saffiotti, U. *Acta Bio-Med. Ateneo Parmense* **2005**, *76*, 30–37.

(13) Melzak, K. A.; Sherwood, C. S.; Turner, R. F. B.; Haynes, C. A. *J. Colloid Interface Sci.* **1996**, *181*, 635–644.

(14) Mercier, P.; Savoie, R. *Biospectroscopy* **1997**, *3*, 299–306.

(15) Fujiwara, M.; Yamamoto, F.; Okamoto, K.; Shiokawa, K.; Nomura, R. *Anal. Chem.* **2005**, *77*, 8138–8145.

(16) Kang, S. H.; Shortreed, M. R.; Yeung, E. S. *Anal. Chem.* **2001**, *73*, 1091–1099.

(17) Li, H.-W.; Park, H.-Y.; Porter, M. D.; Yeung, E. S. *Anal. Chem.* **2005**, *77*, 3256–3260.

(18) Isailovic, S.; Li, H.-W.; Yeung, E. S. *J. Chromatogr.* **2007**, *A1150*, 259–266.

(19) Walter, S. R.; Geiger, F. M. *J. Phys. Chem. Lett.* **2010**, *1*, 9–15.

(20) Sui, J.; Tleugabulova, D.; Brennan, J. D. *Langmuir* **2005**, *21*, 4996–5001.

(21) Lundqvist, M.; Andresen, C.; Christensson, S.; Johansson, S.; Karlsson, M.; Broo, K.; Jonsson, B.-H. *Langmuir* **2005**, *21*, 11903–11906.

(22) Valle-Delgado, J. J.; Molina-Bolívar, J. A.; Galisteo-González, F.; Gálvez-Ruiz, M. J.; Feiler, A.; Rutland, M. W. *Langmuir* **2005**, *21*, 9544–9554.

(23) van der Veen, M.; Norde, W.; Stuart, M. C. *Colloids Surf.* **2004**, *B35*, 33–40.

(24) Dabrowski, J.; Müssig, H.-J. *Silicon Surfaces and Formation of Interfaces: Basic Science in the Industrial World*; World Scientific: River Edge, NJ, 2000.

(25) Yao, S.; Myers, A. M.; Posner, J. D.; Rose, K. A.; Santiago, J. G. *J. Microelectromech. Syst.* **2006**, *15*, 717–728.

(26) Lyklema, J. *Fundamentals of Interface and Colloid Science*; Academic: San Diego, 1991.

(27) Hassanali, A. A.; Singer, S. J. *J. Comput.-Aided Mater. Des.* **2007**, *14*, 53–63.

(28) Hassanali, A. A.; Singer, S. J. *J. Phys. Chem.* **2007**, *B111*, 11181–11193.

(29) As written, the first two terms on the right side of eq 7 in ref 28 involve sums over the silanol oxygens of the silica. They should include a sum over all oxygens of the silica, including both silanol and siloxane types.

(30) Zhang, H.; Hassanali, A. A.; Shin, Y. K.; Knight, C.; Singer, S. J. *J. Chem. Phys.*, in press.

(31) Gouy, M. *Comptes Rendu* **1909**, *149*, 654–657.

(32) Gouy, M. *J. Phys. (Paris)* **1910**, *9*, 457–468.

(33) Chapman, D. L. *Philos. Mag.* **1913**, *25*, 475–481.

(34) Stern, O. *Z. Elektrochem.* **1924**, *30*, 508–516.

(35) Put, A. G. V. D.; Bijsterbosch, B. H. *J. Colloid Interface Sci.* **1983**, *92*, 499–507.

(36) Zukoski, C. F., IV; Saville, D. A. *J. Colloid Interface Sci.* **1986**, *114*, 32–44.

(37) Zukoski, C. F., IV; Saville, D. A. *J. Colloid Interface Sci.* **1986**, *114*, 45–53.

(38) Kijlstra, J.; van Leeuwen, H. P.; Lyklema, J. *J. Chem. Soc., Faraday Trans.* **1992**, *88*, 3441–3449.

(39) Dukhin, S. S. *Adv. Colloid Interface Sci.* **1995**, *61*, 17–49.

(40) Mangelsdorf, C. S.; White, L. R. *J. Chem. Soc., Faraday Trans.* **1998**, *94*, 2441–2452.

(41) Mangelsdorf, C. S.; White, L. R. *J. Chem. Soc., Faraday Trans.* **1998**, *94*, 2583–2593.

(42) Lyklema, J.; Minor, M. *Colloids Surf.* **1998**, *A140*, 33–41.

(43) Dukhin, S. S.; Zimmermann, R.; Werner, C. *Colloids Surf.* **2001**, *A195*, 103–112.

(44) Feuston, B. P.; Garofalini, S. H. *J. Chem. Phys.* **1988**, *89*, 5818–5824.

(45) Feuston, B. P.; Garofalini, S. H. *J. Appl. Phys.* **1990**, *68*, 4830–4836.

(46) Litton, D. A.; Garofalini, S. H. *J. Appl. Phys.* **2001**, *89*, 6013–6023.

(47) Ma, Y.; Garofalini, S. H. *J. Chem. Phys.* **2006**, *124*, 234102.

(48) Mahadevan, T. S.; Garofalini, S. H. *J. Phys. Chem.* **2008**, *C112*, 1507–1515.

(49) Lockwood, G. K.; Garofalini, S. H. *J. Chem. Phys.* **2009**, *131*, 074703.

(50) Mahadevan, T. S.; Garofalini, S. H. *J. Phys. Chem.* **2007**, *B111*, 8919–8927.

(51) Mahadevan, T. S.; Garofalini, S. H. *J. Phys. Chem.* **2008**, *C112*, 5694.

(52) Mahadevan, T.; Garofalini, S. *J. Phys. Chem.* **2009**, *C113*, 11177.

(53) Rustad, J. R.; Hay, B. P. *Geochim. Cosmochim. Acta* **1995**, *59*, 1251–1257.

(54) van Duin, A. C. T.; Strachan, A.; Stewman, S.; Zhang, Q.; Xu, X.; Goddard, W. A. *J. Phys. Chem.* **2003**, *A107*, 3803–3811.

(55) Fogarty, J. C.; Aktulga, H. M.; Grama, A. Y.; van Duin, A. C. T.; Pandit, S. A. *J. Chem. Phys.* **2010**, *132*, 174704.

(56) van Duin, A. C. T.; Dasgupta, S.; Lorant, F.; Goddard, W. A. *J. Phys. Chem.* **2001**, *A105*, 9396–9409.

(57) Cruz-Chu, E. R.; Aksimentiev, A.; Schulten, K. *J. Phys. Chem.* **2006**, *B110*, 21497–21508.

(58) Lamb, R. N.; Furlong, D. N. *J. Chem. Soc., Faraday Trans. 1* **1982**, *78*, 61–73.

(59) Muster, T. H.; Prestidge, C. A.; Hayes, R. A. *Colloids Surf.* **2001**, *A176*, 253–266.

(60) Jenkins, S.; Kirk, S. R.; Persson, M.; Carlen, J.; Abbas, Z. *J. Chem. Phys.* **2007**, *127*, 224711.

(61) Jenkins, S.; Kirk, S. R.; Persson, M.; Carlen, J.; Abbas, Z. *J. Chem. Phys.* **2008**, *128*, 164711.

(62) Jenkins, S.; Kirk, S. R.; Persson, M.; Carlen, J.; Abbas, Z. *J. Chem. Phys.* **2009**, *130*, 134702.

(63) Delley, B. *J. Chem. Phys.* **1990**, *92*, 508–517.

(64) Jorgensen, W. L. In *Encyclopedia of Computational Chemistry*; Schleyer, P. v. R. , Ed.; Wiley: New York, 1998; Vol. 5, pp 3281−3285.

(65) Wensink, E. J. W.; Hoffmann, A. C.; Apol, M. E. F.; Berendsen, H. J. C. *Langmuir* **2000**, *16*, 7392–7400.

(66) Puibasset, J.; Pellenq, R. J.-M. *J. Chem. Phys.* **2003**, *119*, 9226–9232.

(67) Puibasset, J.; Pellenq, R. J.-M. *Phys. Chem. Chem. Phys.* **2004**, *6*, 9226–9232.

(68) Puibasset, J.; Pellenq, R. J.-M. *J. Phys.: Condens. Matter* **2004**, *16*, S5329–S5343.

(69) Puibasset, J.; Pellenq, R. J.-M. *J. Chem. Phys.* **2005**, *122*, 094704.

(70) Puibasset, J.; Pellenq, R. J.-M. *Eur. Phys. J.* **2007**, *ST141*, 41–44.

(71) Lopes, P. E. M.; Murashov, V.; Tazi, M.; Demchuk, E.; Mackerell, A. D., Jr. *J. Phys. Chem.* **2006**, *110*, 2782–2792.

(72) Freund, J. B. *J. Chem. Phys.* **2002**, *116*, 2194–2200.

(73) Qiao, R.; Aluru, N. R. *J. Chem. Phys.* **2003**, *118*, 4692–4701.

(74) Qiao, R.; Aluru, N. R. *Phys. Rev. Lett.* **2004**, *92*, 198301.

(75) Joseph, S.; Aluru, N. R. *Langmuir* **2006**, *22*, 9041–9051.

(76) Lorenz, C. D.; Travesset, A. *Phys. Rev.* **2007**, *E75*, 061202.

(77) Lorenz, C. D.; Crozier, P. S.; Anderson, J. A.; Travesset, A. *J. Phys. Chem.* **2008**, *C112*, 10222–10232.

(78) Some authors (e.g., ref 79) use a water contact angle of 90° as a dividing line between hydrophobic and hydrophilic

surfaces. Others (e.g., ref 80) do not follow a strict convention. Because the experiments of which we are aware[58,59] always report contact angles for unhydroxyated quartz or silica less than 90°, the unhydroxylated silica surface by the fomer convention would still be considered hydrophilic. In this work, we follow the latter convention, and perhaps we should refer to the relative hydrophobicity of siloxanes as compared to silanols.

(79) Giovambattista, N.; Debenedetti, P. G.; Rossky, P. J. *J. Phys. Chem.* **2007**, *111*, 9581–9587.

(80) Israelachvili, J. *Intermolecular and Surface Forces*, 2nd ed.; Academic: San Diego, CA, 1991.

(81) Saengsawang, O.; Remsungnen, T.; Frizsche, S.; Haberlandt, R.; Hannongbua, S. *J. Phys. Chem.* **2005**, *B109*, 5684–5690.

(82) Cheng, H.-P.; Barnett, R. N.; Landman, U. *J. Chem. Phys.* **2002**, *116*, 9300–9304.

(83) Walsh, T. R.; Wilson, M.; Sutton, A. P. *J. Chem. Phys.* **2000**, *113*, 9191–9201.

(84) Konený, R.; Doren, D. J. *J. Chem. Phys.* **1997**, *106*, 2426–2435.

(85) Rimola, A.; Ugliengo, P. *J. Chem. Phys.* **2008**, *128*, 204702.

(86) Criscenti, L. J.; Kubicki, J. D.; Brantley, S. L. *J. Phys. Chem.* **2006**, *A100*, 198–206.

(87) Ma, Y.; Foster, A. S.; Nieminen, R. M. *J. Chem. Phys.* **2005**, *122*, 144709.

(88) Hamad, S.; Bromley, S. T. *Chem. Commun.* **2008**, 4156–4158.

(89) Du, M.-H.; Kolchin, A.; Cheng, H.-P. *J. Chem. Phys.* **2003**, *119*, 6418–6422.

(90) Masini, P.; Bernasconi, M. *J. Phys.: Condens. Matter* **2002**, *14*, 4133–4144.

(91) Mischler, C.; Horbach, J.; Kob, W.; Binder, K. *J. Phys.: Condens. Matter* **2005**, *17* (26), 4005–4013.

(92) Leung, K.; Nielsen, I. M. B.; Criscenti, L. J. *J. Am. Chem. Soc.* **131**, *131*, 18358–18365.

(93) Tielens, F.; Gervais, C.; Lambert, J. F.; Mauri, F.; Costa, D. *Chem. Mater.* **2008**, *20*, 3336–3344.

(94) Tilocca, A.; Cormack, A. N. *ACS Appl. Mater. Interfaces* **2009**, *1*, 1324–1333.

(95) Becke, A. D. *Phys. Rev.* **1988**, *A38*, 3098–3100.

(96) Lee, C.; Yang, W.; Parr, R. G. *Phys. Rev.* **1988**, *B37*, 785–789.

(97) Perdew, J. P.; Burke, K.; Ernzerhof, M. *Phys. Rev. Lett.* **1996**, *77*, 3865–3868.

(98) Grossman, J. C.; Schwegler, E.; Draeger, E. W.; Gygi, F.; Galli, G. *J. Chem. Phys.* **2004**, *120*, 300–311.

(99) Schwegler, E.; Grossman, J. C.; Gygi, F.; Galli, G. *J. Chem. Phys.* **2004**, *121*, 5400–5409.

(100) Kuo, I.-F. W.; Mundy, C. J.; McGrath, M. J.; Siepmann, J. I.; VandeVondele, J.; Sprik, M.; Hutter, J.; Chen, B.; Klein, M. L.; Mohamed, F.; Krack, M.; Parrinello, M. *J. Phys. Chem.* **2004**, *B108*, 12990–12998.

(101) Lee, H.-S.; Tuckermam, M. E. *J. Phys. Chem.* **2006**, *A110*, 5549–5560.

(102) Lee, H.-S.; Tuckerman, M. E. *J. Chem. Phys.* **2006**, *125*, 154507.

(103) Lee, H.-S.; Tuckerman, M. E. *J. Chem. Phys.* **2007**, *126*, 164501.

(104) McGrath, M. J.; Siepmann, J. I.; Kuo, I.-F. W.; Mundy, C. J.; VandeVondele, J.; Hutter, J.; Mohamed, F.; Krack, M. *ChemPhysChem* **2005**, *6*, 1894–1901.

(105) Feuston, B. P.; Garofalini, S. H. *J. Chem. Phys.* **1989**, *91*, 564–570.

(106) Feuston, B. P.; Garofalini, S. H. *J. Phys. Chem.* **1990**, *94*, 5351–5356.

(107) Rustad, J. R.; Wasserman, E.; Felmy, A. R.; Wilke, C. *J. Colloid Interface Sci.* **1998**, *198*, 119–129.

(108) Van Ginhoven, R. M.; Jónsson, H.; Corrales, L. R. *Phys. Rev.* **2005**, *B71*, 24208.

(109) van Beest, B. W. H.; Kramer, G. J.; van Santen, R. A. *Phys. Rev. Lett.* **1990**, *64*, 1955–1958.

(110) Berendsen, H. J. C.; Grigera, J. R.; Straatsma, T. P. *J. Phys. Chem.* **1987**, *91*, 6269–6271.

(111) Møller, C.; Plesset, M. *Phys. Rev.* **1934**, *46*, 618–622.

(112) Bartlett, R. J.; Silver, D. M. *Int. J. Quantum Chem., Symp.* **1974**, *8*, 271–276.

(113) Binkley, J. S.; Pople, J. A. *Int. J. Quantum Chem.* **1975**, *9*, 229–236.

(114) Bartlett, R. J.; Silver, D. M. *Int. J. Quantum Chem., Symp.* **1975**, *9*, 183–198.

(115) Pople, J. A.; Binkley, J. S.; Seeger, R. *Int. J. Quantum Chem., Symp.* **1976**, *10*, 1–19.

(116) Frisch, M. J.; Trucks, G. W.; Schlegel, H. B.; Scuseria, G. E.; Robb, M. A.; Cheeseman, J. R.; Montgomery, J. A., Jr.; Vreven, T.; Kudin, K. N.; Burant, J. C.; Millam, J. M.; Iyengar, S. S.; Tomasi, J.; Barone, V.; Mennucci, B.; Cossi, M.; Scalmani, G.; Rega, N.; Petersson, G. A.; Nakatsuji, H.; Hada, M.; Ehara, M.; Toyota, K.; Fukuda, R.; Hasegawa, J.; Ishida, M.; Nakajima, T.; Honda, Y.; Kitao, O.; Nakai, H.; Klene, M.; Li, X.; Knox, J. E.; Hratchian, H. P.; Cross, J. B.; Bakken, V.; Adamo, C.; Jaramillo, J.; Gomperts, R.; Stratmann, R. E.; Yazyev, O.; Austin, A. J.; Cammi, R.; Pomelli, C.; Ochterski, J. W.; Ayala, P. Y.; Morokuma, K.; Voth, G. A.; Salvador, P.; Dannenberg, J. J.; Zakrzewski, V. G.; Dapprich, S.; Daniels, A. D.; Strain, M. C.; Farkas, O.; Malick, D. K.; Rabuck, A. D.; Raghavachari, K.; Foresman, J. B.; Ortiz, J. V.; Cui, Q.; Baboul, A. G.; Clifford, S.; Cioslowski, J.; Stefanov, B. B.; Liu, G.; Liashenko, A.; Piskorz, P.; Komaromi, I.; Martin, R. L.; Fox, D. J.; Keith, T.; Al-Laham, M. A.; Peng, C. Y.; Nanayakkara, A.; Challacombe, M.; Gill, P. M. W.; Johnson, B.; Chen, W.; Wong, M. W.; Gonzalez, C.; Pople, J. A. *Gaussian 03*, revision C.02; Gaussian, Inc.: Pittsburgh, PA, 2003.

(117) Christen, M.; Hünenberger, P. H.; Bakowies, D.; Baron, R.; Bürgi, R.; Geerke, D. P.; Heinz, T. N.; Kastenholz, M. A.; Kräutler, V.; Oostenbrink, C.; Peter, C.; Trzesniak, D.; van Gunsteren, W. F. *J. Comput. Chem.* **2005**, *26*, 1719–1751.

(118) Dang, L. X. *J. Am. Chem. Soc.* **1995**, *117*, 6954–6960.

(119) Huff, N. T.; Demiralp, E.; Cagin, T.; Goddard, W. A., III. *J. Non-Cryst. Solids* **1999**, *253*, 133–142.

(120) CP2K website, http://cp2k.berlios.de.

(121) VandeVondele, J.; Krack, M.; Mohamed, F.; Parrinello, M.; Chassaing, T.; Hutter, J. *Comput. Phys. Commun.* **2005**, *167*, 103–128.

(122) VandeVondele, J.; Hutter, J. *J. Chem. Phys.* **2003**, *118*, 4365–4369.

(123) Pulay, P. *Chem. Phys. Lett.* **1980**, *73*, 393–398.

(124) Pulay, P. *J. Comput. Chem.* **1982**, *3*, 556–560.

(125) Goedecker, S.; Teter, M.; Hutter, J. *Phys. Rev.* **1996**, *B54*, 1703–1710.

(126) Zhuravlev, L. T. *Pure Appl. Chem.* **1989**, *61*, 1969–1976.

(127) Bakos, T.; Rashkeev, S. N.; Pantiledes, S. T. *Phys. Rev. Lett.* **2002**, *88*, 55508.

(128) Rignanese, G.-M.; Charlier, J.-C.; Gonze, X. *Phys. Chem. Chem. Phys.* **2004**, *6*, 1920–1925.

(129) Blöchl, P. E. *J. Chem. Phys.* **1995**, *103*, 7422–7428.

(130) Peraro, M. D.; Raugei, S.; Carloni, P.; Klein, M. L. *ChemPhysChem* **2005**, *6*, 1715–1718.

(131) Zhu, W.; Singer, S. J.; Zheng, Z.; Conlisk, A. T. *Phys. Rev.* **2004**, *E71*, 041501.

(132) Van de Ven-Lucassen, I. M. J. J.; Vlugt, T. J. H.; Van der Zanden, A. J. J.; Kerkhof, P. J. A. M. *Mol. Phys.* **1998**, *94*, 495–503.

(133) Chen, T.; Smit, B.; Bell, A. T. *J. Chem. Phys.* **2009**, *131*, 246101.

(134) Marry, V.; Dufreche, J.-F.; Jardat, M.; Meriguet, G.; Turq, P.; Grun, F. *Colloids Surf.* **2003**, *A222*, 147–153.

(135) Dufreche, J.-F.; Marry, V.; Malíková, N.; Turq, P. *J. Mol. Liq.* **2005**, *118*, 145–153.

CT100260Z